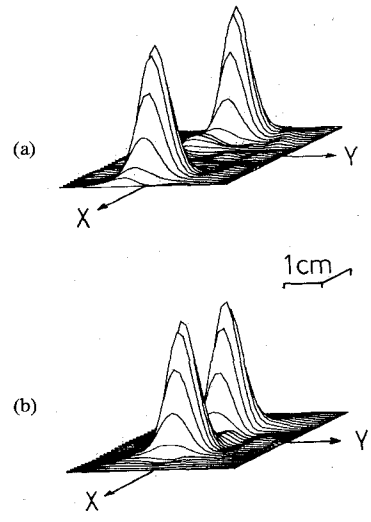

Fig. 4. Rods equivalent currents (cross section) as function of separation. (a) $d = 2.4\,\lambda$ (27.8 mm); (b) $d = 1.2\,\lambda$ (13.9 mm).

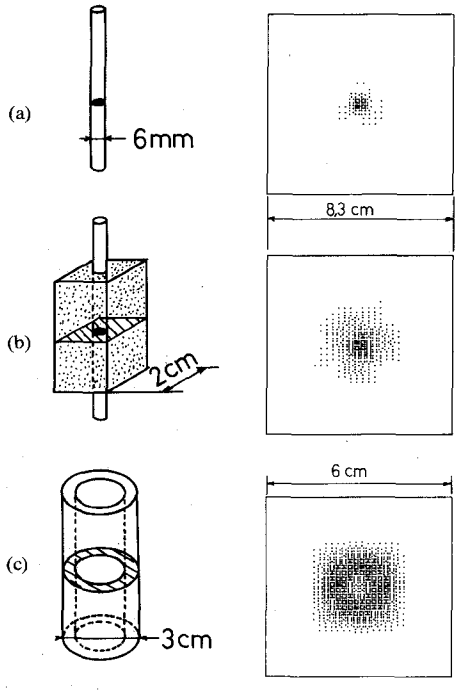

Fig. 5. Equivalent currents of dielectric bodies (cross section) in the case of four orthogonal illuminations. (a) Rod. (b) Rod surrounded by sponge. (c) Water filled plexiglas cylinder.

Fig. 5 shows three examples of various dielectric cylinders reconstruction using four orthogonal measurements.

As an indication of measurement speed, recording the field on a measurement line requires approximately one half of a second; the time required for deducing the graphs of Fig. 4 is 50 s on a HP 1000 with use of FTT algorithms but without any special processor.

VI. Conclusion

This short paper shows the possibility of fast coherent tomography of biological media. In contradistinction to conventional computerized tomography, the algorithms take into account diffraction effects. The organs are viewed from their equivalent currents which depend both from the permittivity and from the illuminating field. Numerical simulations are in progress in order to estimate the usefulness of such a representation and the contrasts to be expected. The modulation scattering technique allows amplitude-phase recording at the rate of a few milliseconds per point. The sensitivity of the receiver is sufficient for atraumatic illumination levels, always less than 10 mW/cm^2. Multiple illuminations provide a spatial resolution of $\lambda/2$ where λ is the wavelength in water ($\lambda = 1.16$ cm at 3 GHz).

Acknowledgment

The authors wish to thank the Laboratoire de Thermologie Biomedicale (Strasbourg) and Société d'Etude du Radant (Orsay) for their collaboration in this work.

References

[1] L. E. Larsen and J. H. Jacobi, "Microwave scattering imagery of isolated canine kidney," *Med. Phys.*, vol. 6, pp. 394–403, 1979.
[2] J. H. Jacobi and L. E. Larsen, "Microwave time-delay spectroscopic imagery of isolated canine kidney," *Med. Phys.*, vol. 7, pp. 1–7, 1980.
[3] H. Ermert, F. Fülle, and D. Hiller, "Microwave computerized tomography," in *Proc. 11th Euro. Microwave Conf.*, (Amsterdam) 1981, pp. 421–426.
[4] J. J. Stamnes, "Focusing of two-dimensional waves," *J. Opt. Soc. Amer.*, vol. 71, no. 1, pp. 15–31, 1981.
[5] M. F. Adams and A. P. Anderson, "Three dimensional image-construction technique and its application to coherent microwave diagnostics," in *Inst. Elec. Eng. Proc.*, vol. 127, 1980, pp. 138–142.
[6] J. Ch. Bolomey, "La méthode de diffusion modulée: Une approche au relevé des cartes de champs électromagnétiques en temps réel," Inv. Com., Reunion anual de la Comission B, Comité espagnol de la URSI, Barcelona, Oct. 1–2 1981, p. XI. Published in *l'Onde Electrique*, May 1982.
[7] J. H. Richmond, "A modulated scattering technique for measurement of field distribution," *IRE Trans.*, vol. 3, pp. 13–18, 1965.
[8] M. Leroy, "Simple and efficient amplitude-phase receiver to measure the electromagnetic fields by the modulated scattering technique," Groupe d'Electromagnétisme, Tech. Rep. R77-28.
[9] R. K. Mueller, M. Kaveh, and R. D. Iverson, "A new approach to acoustic tomography using diffraction techniques," in *Acoustic Holography*, vol. 8, A. Metherell, Ed. New York: Plenum Press, 1978.
[10] D. E. Livesay and K. M. Chen, "Electromagnetic fields induced inside arbitrarily shaped biological bodies," *IEEE Trans. Microwave Theory Tech.*, vol. MTT-22, pp. 1273–1280, Dec. 1974.
[11] Ch. Pichot, L. Jofre, G. Peronnet, A. Izadnegahdar, and J. Ch. Bolomey, "An angular spectrum method for inhomogeneous bodies reconstruction in microwave domain," presented at IEEE/AP-S and URSI Symp., Albuquerque, May 24–28, 1982.

Numerical and Experimental Results for Near-Field Electromagnetic Absorption in Man

I. CHATTERJEE, MEMBER, IEEE, O. P. GANDHI, FELLOW, IEEE, AND M. J. HAGMANN, MEMBER, IEEE

***Abstract*—Experimental results are presented for the whole-body-average energy absorption and the internal *E*-fields in man exposed to leakage-type near fields. An empirical relationship, previously presented [1]**

Manuscript received January 6, 1982; revised May 18, 1982. This work was supported in part by the National Institute of Environmental Health Sciences, Research Triangle Park, NC, under Grant ES02304.

I. Chatterjee and O. P. Gandhi are with the Department of Electrical Engineering, University of Utah, Salt Lake City, UT 84112.
M. J. Hagmann was with the University of Utah, and is presently with the Department of Electrical Engineering, University of Hawaii, Honolulu, HI.

0018-9480/82/1100-2000$00.75 ©1982 IEEE

for whole-body-average energy absorption in man exposed to near fields with *P*-polarization (no component of *E* arm-to-arm) is extended to near fields with *N*-polarization (*E* arm-to-arm). The empirical and experimental results are in good agreement and demonstrate that the internal *E*-fields and the energy absorption for near-field partial-body exposures are considerably smaller than those obtained for plane waves with incident electric field commensurate with the maximum *E*-field used for near-field exposures. The effect of an infinite perfectly conducting ground plane is presented for a limited number of cases.

I. Introduction

Near-zone exposure of humans to electromagnetic fields is of significance in many industrial environments. The calculation and the measurement of electromagnetic energy absorption in humans for near-field exposure conditions are particularly important because of the very high strengths of leakage fields (electric fields on the order of 200–1000 V/m and magnetic fields of 0.2–2.0 A/m) from industrial RF heat sealers and other occupational uses of RF equipment [2], [3].

An empirical relationship has been previously presented [1] for the mass-normalized whole-body-average electromagnetic energy (SAR) in a 180-cell block model of man for near-field exposure conditions. Consideration was restricted to leakage-type near-fields with *P*-polarization (no component of *E*-field directed arm-to-arm) and which exhibited a rolloff to negligible values in the vertical and horizontal directions over a vertical plane just in front of the feet of the block model. The magnitude of the incident *E*-field was maximum immediately in front of the abdominal region of the model. This placement of the *E*-field with respect to the block model was chosen because, except at frequencies corresponding to strong part-body resonances, it is the one which results in maximum whole-body-average SAR.

We have extended this empirical relationship to include *E*-fields with *N*-polarization (*E* arm-to-arm). The relative importance of near-zone electromagnetic field orientation for calculating the SAR in the block model has been evaluated over the frequency range 10–915 MHz. It is deemed necessary to include the contributions of *P*- and *N*-polarizations in estimating the whole-body-average SAR, since the fields in general will consist of components with both polarizations. The contribution of the *N*-polarized field components to the total SAR is important only at frequencies greater than about 100 MHz.

Experiments have been performed with reduced-scale figurines of various sizes, filled with saline, for estimating the whole-body-average SAR. Measurements have also been made of the internal *E*-field magnitude in the abdominal region of the figurines, filled with biological tissue-simulating materials.

The near-field SAR has been calculated for a limited number of cases when the block model is in perfect contact with an infinite perfectly conducting ground plane as well as when there is a small separation from the ground plane.

II. The Empirical Relationship for *P*- and *N*-Polarization and the Relative Importance of Near-Field Orientation

The empirical relationship for the whole-body-average SAR in the 180-cell block model of man presented in a previous paper [1] for near-field exposure conditions is given by (1)

$$\mathrm{SAR}|_{\text{near-field}} = \frac{\mathrm{SAR}|_{\text{far-field}}}{\left[1+\left(\frac{A_h}{\Delta_h}\right)^2\right]\left[1+\left(\frac{A_v}{\Delta_v}\right)^2\right]}. \quad (1)$$

Consideration was restricted at that time to near fields with *P*-polarization. Here, Δ_h and Δ_v are the physical extents of the best-fit half-cycle cosine functions to the incident vertical *E*-field component in the horizontal and vertical directions, respectively, over a plane just in front of the feet of the model.

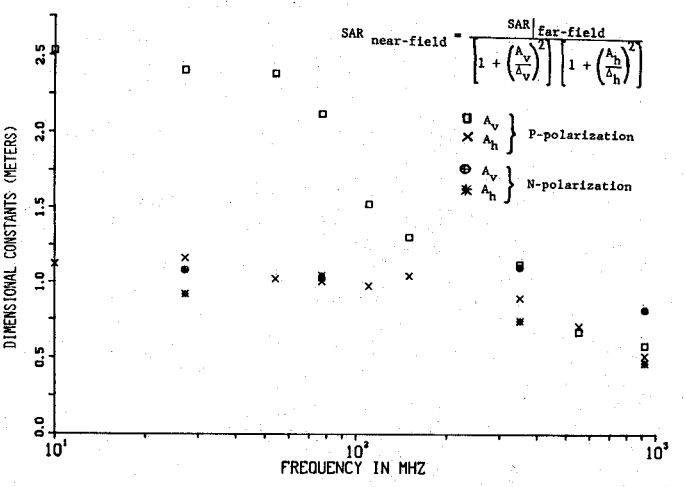

Fig. 1. Dimensional constants for the near-field empirical relationship for *P*- and *N*-polarizations.

Equation (1) was based on numerical results which indicated that for small values of Δ_h and Δ_v ($\ll \lambda$, where λ is the free-space wavelength) the near-field SAR varied as $(\Delta_v^2 \Delta_h^2/\lambda^4)$ [4]. The empirical relationship also reduces to the far-field values for large values of Δ_h and Δ_v ($> \lambda$). A_h and A_v are dimensional constants obtained by matching to the limiting behavior of the near-field SAR for small values of Δ_h and Δ_v. Fields encountered in practice generally consist of components with both *P*- and *N*-polarizations. It is necessary, therefore, to extend calculations to fields with *N*-polarization to see if an empirical relationship can also be obtained in this case.

Numerical calculations of the whole-body-average SAR for the 180-cell block model exposed to near-fields with *N*-polarization and having a half-cycle cosine variation in the vertical and horizontal directions predicted (1) to be still valid. The corresponding values of A_h and A_v are plotted in Fig. 1 for both *N*- and *P*-polarizations, for various frequencies from 10 to 915 MHz.

It was pointed out in [1] that for *P*-polarization, A_h and A_v are relatively constant for frequencies below whole-body resonance (77 MHz for the block model). These values of A_v and A_h are approximately 2.5 m and 1.1 m, corresponding to 1.4 times the height and 2.1 times the width of the block model, respectively. The SAR given by (1) for field distributions considerably broader than the physical dimensions of the block model ($\Delta_v \gg 1.75$ m, $\Delta_h \gg 0.53$ m) is the far-field value. The values of A_v and A_h at frequencies below whole-body resonance for the case of *N*-polarization (Fig. 1) are both approximately 1 m. This is because, for this polarization, little deposition is obtained in the vertical extremities (head, neck, and legs) of the block model and most of the deposition is in the torso and arms. This behavior has also been previously reported for far-field irradiation conditions [5]. The far-field SAR value is obtained for $\Delta_v, \Delta_h \gg 1$ m; that is, as long as the field distribution is fairly constant over the extent of the torso and arms. Hence

$$A_v|_{N\text{-polarization}} < A_v|_{P\text{-polarization}}$$

at low frequencies.

The dimensional constants A_v and A_h are comparable between themselves as well as for the two polarizations at frequencies higher than 200–250 MHz. A point to note is that for both *P*- and *N*-polarizations, the near-field SAR is considerably lower than the SAR for whole-body far-field exposure conditions, when

TABLE I
WHOLE BODY-AVERAGE SAR FOR SALINE-FILLED FIGURINES UNDER NEAR-FIELD EXPOSURE CONDITIONS. EXPERIMENTAL FREQUENCY = SIMULATED FREQUENCY × (HEIGHT OF MAN/HEIGHT OF FIGURINE)

Simulated Frequency for Man (MHz)	Model Size (cm)	Experimental Frequency (MHz)	Physical Parameters for the Fields at the Simulated Frequency (Meters)		Average SAR (±Standard Deviation) μW/kg for Maximum E_v = 1 V/m rms		SAR for Plane-Wave Irradiation (μW/kg)*
			Δ_v †	Δ_h †	Experimental‡ N = 5	Empirical Equation	
71	20.3	610	.412	1.28	1.0 (±.029)	1.2	58.4
77	20.3	663	.484	1.32	1.7 (±.029)	1.8	58.6
88	20.3	760	.622	1.66	2.6 (±.081)	3.8	52.0
96	25.4	663	.388	1.06	1.4 (±.075)	1.3	48.0
110	25.4	760	.496	1.32	2.0 (±.067)	2.4	39.2
115	33.0	610	.212	.657	.42 (±.064)	.46	36.0
125	33.0	663	.298	.814	.66 (±.045)	.58	33.4
143	33.0	760	.256	.816	.38 (±.040)	.46	35.0
150	33.0	795	.276	.742	.54 (±.0035)	.42	26.0
176	40.6	760	.207	.690	.20 (±.050)	.19	22.6

† Obtained by measurement.

‡ Average of three measurements; standard deviation less than ±5 percent, calculated from 4180ΔT/(irradiation time in seconds)[6].

* Obtained numerically.

the physical extents Δ_v and Δ_h are much less than A_v and A_h, respectively.

The empirical results for near-field exposures also predict that for frequencies up to and slightly exceeding the whole-body resonance frequency (77 MHz), the SAR due to fields with *N*-polarization is negligible compared to the SAR due to fields with *P*-polarization for identical physical extents Δ_h and Δ_v. This is because the far-field SAR which appears in the numerator of (1) in the case of *N*-polarization is less than in the case of *P*-polarization by about an order of magnitude. The SAR's due to near-fields with *P*- and *N*-polarization having identical physical extents Δ_v and Δ_h are comparable at frequencies above about 100 MHz.

Measurements of leakage ***E***-fields in front of RF dielectric heat sealers have indicated that the *P*-polarized components of the ***E***-field are the dominant ones, and, therefore, the contribution of the *N*-polarized component to the whole-body-average SAR is relatively negligible. The contributions of both polarizations to the total SAR must, however, be included in cases where both the *P*- and *N*-polarized ***E***-field components are comparable such as at frequencies above about 100 MHz.

III. EXPERIMENTAL RESULTS

The experimental arrangement is shown in Fig. 2. Leakage fields similar to those from an RF heat sealer were simulated on a reduced scale by means of a parallel-plate applicator. The applicator consisted of metal plates of dimensions 7×7 cm separated by a 1-cm thickness of Styrofoam. Power (40–80 W) from an MCL RF power generator (model 15122) was used to excite the plates. Bulk of the power was reflected back from the plates since the plate dimensions were much smaller than the wavelength. This resulted in only fringing fields being present in front of the plates, simulating the leakage fields in front of an RF sealer. The reflected power was transferred to a high-power termination via a circulator.

A. Whole-Body-Average SAR

The validity of the empirical relationship ((1)) for whole-body average SAR was tested experimentally. Reduced-scale figurines of four different sizes were filled with saline to simulate man at

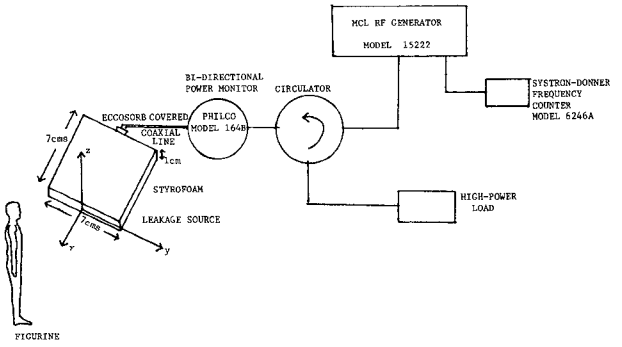

Fig. 2. Experimental arrangement for near-field exposure.

frequencies between 70 and 180 MHz. The saline had a conductivity equal to two-thirds the scaled conductivity of wet tissue at the scaled experimental frequency, since man is considered to consist, on the average, of two-thirds wet tissue. Various extents Δ_v and Δ_h [1] of the vertical ***E***-field were used to test the empirical relationship.

The figurines were exposed to the leakage fields from the applicator for a time interval of 12 min. The temperatures before and after irradiation were measured by means of a digital thermometer (Bailey Instruments Inc., model BAT-8) after the figurine had been thoroughly shaken in order to equalize the temperature over the volume of the saline. The whole-body-average SAR in W/kg for the figurine was calculated from the expression (4180 $\Delta T\times$ specific heat of the wet tissue in calories/(gm°C)/irradiation time in seconds), where ΔT was the measured increase in temperature [6]. This was divided by the figurine scaling factor to obtain the SAR for man.

The values of the whole-body-average SAR obtained experimentally are shown in Table I. The corresponding values obtained from the empirical relationship, as well as the SAR's for plane waves, are also shown for an incident field of rms magnitude 1 V/m. Good agreement is seen between the experimental

[1] Δ_v and Δ_h are equal to twice the vertical and horizontal distance, respectively, between the points where the vertical ***E***-field has a value equal to 0.707 times its maximum value. The extents Δ_v and Δ_h were caused to vary by changing the distance of the figurine from the applicator plates.

TABLE II
INTERNAL ELECTRIC FIELD IN THE ABDOMINAL REGION OF BIOLOGICAL PHANTOM-FILLED FIGURINES AS A FRACTION OF THE MAXIMUM INCIDENT ELECTRIC FIELD (JUST IN FRONT OF THE FIGURINE) FOR NEAR-FIELD EXPOSURE CONDITIONS

Simulated Frequency for Man (MHz)	Figurine Size (cm)	Experimental Frequency (MHz)	Δ_v/λ	Δ_h/λ	Internal $\|\vec{E}\|$/Incident $\|E_v\|$† Near Field		
					Experimental*	Numerical**	Far Field** (Numerical)
77	25.4	530	.18	.40	.070	.070	.42
77	20.3	663	.16	.40	.049	.059	.42
110	25.4	760	.18	.43	.033	.060	.29
150	40.6	663	.09	.30	.022	.025	.14
150	33.0	795	.10	.45	.040	.042	.14

† BRH electric-field probes were used for internal and external field measurements (courtesy of Howard Bassen).

* Average of three measurements, standard deviation less than 5 percent.

** Obtained by averaging calculated values of $|\vec{E}|$ for the abdominal cells of the 180-cell block model of man.

and empirical results. The important point to note is that for a prescribed value of the maximum *E*-field, the near-field SAR's, particularly for $\Delta_h < A_h$ and $\Delta_v < A_v$, are considerably lower than the corresponding SAR's for plane waves.

B. Internal *E*-Field

The local values of the magnitude of the internal *E*-field in the abdominal region of the reduced-scale figurines were measured. The figurines were filled with biological tissue-simulating materials which consisted of mixtures containing water, polyethylene powder, Superstuff[2] (a gelling agent), and salt [7]. The proportions of these constituents were such as to obtain a complex permittivity at the experimental frequencies close to two-thirds the respective values of the high-water content tissues at the lower, simulated frequencies.

The three frequencies (77, 110, and 150 MHz) were simulated for man. The magnitude of the internal *E*-field in the abdominal region of the figurines was measured using the single-axis BRH/NARDA implantable probe[3] (BRH model 13). This probe incorporated a short insulated dipole of length 1.5 mm, and the entire tip size of the probe was 1 mm by 2 mm. A nonperturbing fiber optic cable linked the probe's optical telemetry system to a digital receiver. The probe was calibrated over a range of frequencies in tissue equivalent spheres irradiated by plane waves [8]. The probe's sensitivity allowed internal field strengths of 9–80 V/m to be measured in wet tissue.

Table II shows the measured values of the internal *E*-field magnitude as a fraction of the maximum incident *E*-field for various values of Δ_v and Δ_h. The corresponding numerically calculated values for the 180-cell block model are also shown, together with the calculated values for far-field exposures. Good agreement is seen between the measured and experimental results. The important points to note in Table II are as follows.

a) The internal *E*-field magnitude is less than the incident *E*-field by greater than an order of magnitude.
b) The internal *E*-field ratio in the case of near-field exposure is less than that obtained for far-field exposure by a factor of 3 or more.

The internal *E*-field magnitude for far-field exposure was measured only at the experimental frequency of 370 MHz, due to limitations on the availability of equipment for setting up a far-field exposure system at the other scaled experimental frequencies.[4] A reduced-scale figurine of size 25.4 cm was used to simulate man at a frequency of 54 MHz. The internal *E*-field magnitude in the abdominal region of the figurine as a fraction of the maximum incident *E*-field was measured to be 0.263. This is in fairly good agreement with the value 0.291 calculated for the inhomogeneous block model under far-field exposure conditions.

The slight discrepancy between the sets of calculated and experimental values both in Tables I and II may be due to the fact that the 180-cell block model had inhomogeneous permittivities, whereas the figurines had a homogeneous permittivity. Inhomogeneous modeling of the figurines is impractical and was therefore not undertaken. The spatial integrative method of calculating the whole-body-average SAR, however, results in good agreement between the two sets of values in Table I.

In all the above experiments, the *E*-field in front of the applicator over a vertical plane just in front of the feet of the figurine was measured using the BRH isotropic free-space *E*-field probe which incorporated three orthogonal dipoles with individual outputs to measure the three vector components of the *E*-field.[5]

IV. EFFECT OF AN INFINITE PERFECTLY CONDUCTING GROUND PLANE

The change in the whole-body-average SAR of the block model, due to the presence of an infinite, perfectly conducting ground plane was studied numerically for a few cases of most relevance in real life.

The leakage *E*-field was measured in front of a 27.12 MHz RF heat sealer with a 84-cm×72-cm base plate, set up in our laboratory by Robert Curtis of OSHA. The screen room in which this sealer was situated had a built-in ground plane. The whole-body-average SAR in the block model standing on an infinite, perfectly conducting ground plane, exposed to this measured

[2] Obtained from Oil Center Research, Lafayette, LA.
[3] Courtesy of Howard Bassen of the Bureau of Radiological Health.
[4] An MCL RF power amplifier (model 10110B), having a frequency range 200–400 MHz, was the only one available in our laboratory.
[5] Courtesy of Howard Bassen of the Bureau of Radiological Health.

TABLE III
CALCULATED WHOLE-BODY-AVERAGE AND PART-BODY SAR'S FOR MAN IN THE PRESENCE OF AN INFINITE, PERFECTLY CONDUCTING GROUND PLANE

Frequency = 27.12 MHz

Calculated SAR in μW/kg for a spatial maximum in vertical $\dot{E}$-field = 1 V/m rms

	Incident Fields Corresponding to Those of an RF Sealer*			General Half-Cycle Cosine Distribution of the Incident Fields		
	Perfect Contact with Ground Plane	5 cm Separation from Ground Plane	Absence of Ground Plane	Perfect Contact with Ground Plane	5 cm Separation from Ground Plane	Absence of Ground Plane
Whole-body-average	.320	.038	.044	29.6	5.1	2.3
Torso	.039	.0068	.037	6.6	2.5	1.4
Head	.018	.0033	.025	4.9	2.5	1.5
Neck	.046	.0086	.066	12.3	6.0	3.6
Leg	1.0	.028	.069	86.2	12.2	4.6
Arm	.0018	.00031	.021	.78	.52	.37

* As measured with the participation of Robert Curtis of OSHA.

E-field was calculated in the following two cases: a) perfect contact of the model with the ground plane, and b) a separation of 5 cm of the model from the ground plane.

In both cases, the presence of the ground plane was accounted for by imaging the block model and the *E*-field in the ground plane so that the boundary condition that the tangential *E*-field is zero at the ground plane was satisfied. Similar calculations were also performed for a more general case where imaging the *E*-field, which had a half-cycle cosine function variation (in the absence of the ground plane), produced a peak in the vertical *E*-field component at the ground plane. The case where this peak at the ground plane was equal in magnitude to the spatial peak of the *E*-field in the absence of the ground plane was considered. The results are summarized in Table III. The important points to note are as follows.

1) The SAR's in the case of the RF sealer fields are less than the SAR's in the case of the more general field, with half-cycle cosine variation, by greater than an order of magnitude. This is because, in the latter case, the field considered had a wider extent Δ_v in the vertical direction than the RF sealer field in order to produce a second peak at the ground plane in which it was imaged.

2) In the case of the RF sealer fields, there is a negligible difference between the whole-body-average SAR obtained in the absence of the ground plane and that obtained in the presence of the ground plane with the block model separated from it by 5 cm. Similar observations have been previously made for the case of plane-wave exposures [9], [10]. The whole-body-average SAR of the block model in perfect contact with the ground plane is greater than the SAR of the model separated by 5 cm from the ground plane by a factor of about 8.5.

3) The whole-body-average SAR of the block model in perfect contact with the ground plane is greater than the SAR of the model separated by 5 cm from the ground plane by a factor of about 6 for the more general half-cycle cosine variation of the incident *E*-field. The SAR when the model is separated by 5 cm from the ground plane is not quite equal to the SAR in the absence of the ground plane. A larger separation from the ground plane would be necessary in order that the SAR when the model is not in contact with the ground plane be equal to the SAR in the absence of the ground plane.

We can conclude from the above that in some cases, when the incident field distributions are wide, the effect of the ground plane separated from the model by 5 cm may not be entirely negligible. The numerical calculation of the SAR in such cases would have to consider the presence of the images of the block model and the incident *E*-field in the ground plane. The effect of the ground plane can, however, be neglected in cases like the RF sealer *E*-fields and the whole-body-average SAR calculated using the empirical relationship ((1)).

V. CONCLUSIONS

An empirical relationship, previously presented for the whole-body-average SAR in the 180-cell block model of man for *P*-polarized near fields, has been extended to *N*-polarized near fields. The contribution of the *N*-polarized field components to the total SAR is important only at frequencies greater than about 100 MHz. Experimental results using reduced-scale figurines for the whole-body-average SAR are in good agreement with the results obtained from the empirical relationship. Measured internal *E*-fields in the figurines are in good agreement with the internal *E*-fields obtained numerically. The highlight of these results is that for near-field leakage-type exposures, the internal *E*-fields and hence the SAR's are considerably smaller than those for far-field exposure conditions.

The effect of an infinite, perfectly conducting ground plane on the whole-body-average SAR is negligible in the case of exposure to RF sealer leakage fields when the block model is separated from the ground plane by 5 cm. A larger separation from the ground plane may be required for wider incident field distributions for the same conclusion to be true.

ACKNOWLEDGMENT

The authors wish to acknowledge the assistance of T. Thimakis in obtaining part of the experimental data.

REFERENCES

[1] I. Chatterjee, M. J. Hagmann, and O. P. Gandhi, "An empirical relationship for electromagnetic energy absorption in man for near-field exposure conditions," *IEEE Trans. Microwave Theory Tech.*, vol. MTT-29, pp. 1235–1238, Nov. 1981.

[2] D. L. Conover, W. E. Murray, Jr., E. D. Foley, J. M. Lary, and W. H Parr, "Measurement of electric- and magnetic-field strengths from industrial radio-frequency (6–38 MHz) plastic sealers," *Proc. IEEE*, vol.

68, pp. 17–24, 1980.
[3] K. H. Mild, "Occupational exposure to radio-frequency electromagnetic fields," *Proc. IEEE*, vol. 68, pp. 12–17, 1980.
[4] I. Chatterjee, M. J. Hagmann, and O. P. Gandhi, "Electromagnetic energy deposition in an inhomogeneous block model of man for near-field irradiation conditions," *IEEE Trans. Microwave Theory Tech.*, vol. MTT-28, pp. 1452–1459, 1980.
[5] O. P. Gandhi, "Dosimetry—The absorption properties of man and experimental animals," *Bull. N.Y. Acad. Med.*, Second Series, vol. 55, pp. 999–1020, 1979.
[6] O. P. Gandhi, K. Sedigh, A. S. Beck, and E. L. Hunt, "Distribution of electromagnetic energy deposition in models of man with frequencies near resonance," *Biological Effects of Electromagnetic Waves*, selected papers of the 1975 USNC/URSI meeting, Boulder, CO, vol. II, pp. 44–67 [HEW Publication (FDA) 77-8011].
[7] O. P. Gandhi and K. Sedigh, "Biological phantom materials for simulating man at different frequencies," presented at the 1976 USNC/URSI Meeting, Amherst, MA, Oct. 11–15, 1976.
[8] H. Bassen, P. Herchenroeder, A. Cheung, and S. Neuder, "Evaluation of an implantable electric field probe within finite simulated tissues," *Radio Sci.*, vol. 12, pp. 15–25, 1977.
[9] M. J. Hagmann and O. P. Gandhi, "Numerical calculation of electromagnetic energy deposition in models of man with grounding and reflector effects," *Radio Sci.*, vol. 14, no. 6S, pp. 23–29, 1979.
[10] C. H. Durney *et al.*, *Radiofrequency Radiation Dosimetry Handbook*, 2nd ed., Departments of Electrical Engineering and Bioengineering, University of Utah, Salt Lake City, UT 84112, 1978, pp. 26–29.

Open-Ended Circular Waveguide with a Curved Corrugated Disk at its Aperture as a Diathermy Applicator

PERAMBUR S. NEELAKANTASWAMY
AND ARTHUR RAJARATNAM

Abstract—**A direct-contact type of diathermy applicator consisting of an open-ended circular waveguide loaded with a curved (concave) corrugated disk at its aperture is described. The waveguide is dimensioned to support the dominant TE_{11} mode. Performance characteristics of this applicator are compared with those of an identical structure having a flat corrugated disk at the aperture rim [1]. Also, the superiority of the proposed applicator in respect of improved beam symmetry and reduced edge-diffraction effect (leakage) is indicated. Experimental results on the near-field distributions in the principal planes of a test applicator are presented and are compared with relevant results obtained from a flat-disk loaded applicator [1] of identical dimensions. Also, to get improved input VSWR performance (VSWR less than 1.6), off-setting the corrugated disk (flat or curved) behind the aperture is suggested and is also demonstrated experimentally. Furthermore, as a design flexibility and to simplify fabrication, filling the corrugation grooves with a suitable dielectric material is suggested and explained. Lastly, the feasibility of using a simple corrugated circular waveguide as an alternative direct-contact type of applicator is discussed.**

I. Introduction

Stuchly *et al.* [1] presented a design method and experimental results for a direct-contact circular-aperture diathermy applicator consisting of an open-ended circular waveguide flanged with a flat corrugated disk at its open end [1, fig. 2]; and they effectively demonstrated its acceptable performance in respect to uniform heating patterns, low power leakage, good beam symmetry, compactness of the structure, and low input VSWR at *X*- and *S*-band frequencies.

Manuscript received March 4, 1982; revised April 27, 1982.
The authors are with the Department of Physics, Faculty of Science, National University of Singapore, Kent Ridge, Singapore 0511, Republic of Singapore.

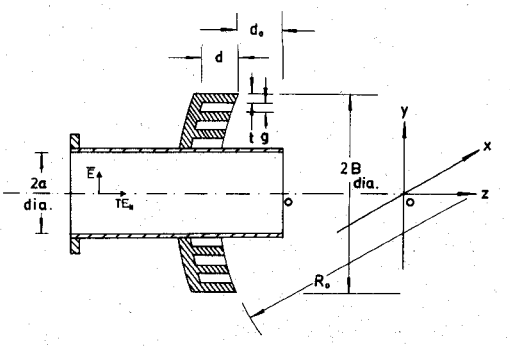

Fig. 1. Direct-contact applicator formed by a circular waveguide with a curved (concave) corrugated flange kept off-set behind the waveguide aperture. Frequency 9.47 GHz. Dimensional details: $2a = 25$ mm; $t = 2.0$ mm; $g = 2.0$ mm; $2B = 53$ mm; $R_0 = 150$ mm; Depth of corrugations d: 8.2 mm without dielectric and 4.9 mm with dielectric. (Dielectric used: Paraffin wax, $\epsilon_r = 2.73$). Off-set distance d_o is adjustable for minimum input VSWR.

The structure described in [1] is well known in antenna engineering as a primary feed with the designation "corrugated conical horn with 90° flare angle" [2],[3]. These radiators, in general, exhibit a good beam symmetry and low edge leakage (that is, side-lobe power) by virtue of quarter-wave choke action caused by the grooves of the corrugations [3]. However, the full benefits of these structures are realized only if the diameter $2B$ of the corrugated disk is much larger than the wavelength λ [4]. Otherwise, a disk of small diameter having a few corrugations would not suppress the edge fields effectively, with the result that edge-diffracted secondary field components may still be present, causing asymmetry in the main lobe with a distorted *E*-plane pattern and power leakage through side lobes in the forward and back regions of the aperture plane [5].

When this type of radiator is used as direct-contact diathermy applicators as suggested in [1], the diameter of the corrugated disk should be kept small in order to make the unit compact and light weighted; hence, only a few (2 to 4) corrugations on the disk is desirable. It means, therefore, that only a partial suppression of edge field could be realized.

In the present work, a modification to the applicator of [1] is suggested so as to realize almost a complete suppression of edge effects in spite of the diameter of the corrugated disk being small. The proposed modification is to replace the flat corrugated disk at the waveguide aperture by a curved (concave) one [6]–[9], as illustrated in Fig. 1. Relevant improvements in the performance characteristics of this modified structure are studied here in detail.

II. Description of the Proposed Structure and Design Considerations

Referring to Fig. 1, an open-ended circular waveguide is loaded with a curved corrugated disk at its aperture end. The inner diameter of the circular waveguide $2a$ is such that, the dominant (TE_{11}) mode at the working frequency alone propagates in it. The groove depth d of corrugations is made to be greater than a quarter of the wavelength λ so that surface waves are eliminated. The groove width g and the tooth width t of the corrugations are dimensioned to get a fairly large corrugation density (that is, a number of corrugations per wavelength). The diameter of the corrugated disk $2B$ is made to be less than twice the wavelength so the structure is compact enough to be used as a direct-contact applicator. In Fig. 1, the disk consists of three corrugations.

The radius of curvature R_0 of the corrugated disk is chosen to be approximately five times the wavelength, which ensures no

0018-9480/82/1100-2005$00.75 ©1982 IEEE